

1 **Meteorological characteristics of extreme ozone pollution events**
2 **in China and their future predictions**

3
4
5
6 Yang Yang^{1*}, Yang Zhou², Hailong Wang³, Mengyun Li¹, Huimin Li¹, Pinya Wang¹, Xu Yue¹,
7 Ke Li¹, Jia Zhu¹, Hong Liao¹

8
9
10 ¹Joint International Research Laboratory of Climate and Environment Change, Jiangsu Key
11 Laboratory of Atmospheric Environment Monitoring and Pollution Control, Jiangsu
12 Collaborative Innovation Center of Atmospheric Environment and Equipment Technology,
13 School of Environmental Science and Engineering, Nanjing University of Information
14 Science and Technology, Nanjing, Jiangsu, China

15 ²Shanghai Baoshan Meteorology Bureau, Shanghai, China

16 ³Atmospheric Sciences and Global Change Division, Pacific Northwest National Laboratory,
17 Richland, WA, USA

18
19
20
21
22 *Correspondence to yang.yang@nuist.edu.cn

23 **Abstract**

24 Ozone (O₃) has become one of the most concerning air pollutants in China in recent
25 decades. In this study, based on surface observations, reanalysis data, global atmospheric
26 chemistry model simulations and multi-model future predictions, meteorological
27 characteristics conducive to extreme O₃ pollution in various regions of China are investigated,
28 and their historical changes and future trends are analyzed. During the most severe O₃ polluted
29 months, the chemical production of O₃ is enhanced under the hot and dry conditions over the
30 North China Plain (NCP) in June 2018 and Yangtze River Delta (YRD) in July 2017, while the
31 regional transport is the main reason causing the severe O₃ pollution over Sichuan Basin (SCB)
32 in July 2015 and Pearl River Delta (PRD) in September 2019. Over the last four decades, the
33 frequencies of high temperature and low relative humidity conditions increased in 2000-2019
34 relative to 1980-1999, indicating that O₃ pollution in both NCP and YRD became more frequent
35 under the historical climate change. In SCB and PRD, the occurrence of atmospheric
36 circulation patterns similar to those during the most polluted months increased, together with
37 the more frequent hot and dry conditions, contributing to the increases in severe O₃ pollution
38 in SCB and PRD during 1980–2019. In the future (by 2100), the frequencies of months with
39 anomalous high temperature show stronger increasing trends in the high forcing scenario
40 (SSP5-8.5) compared to the sustainable scenario (SSP1-2.6) in China. It suggests that high
41 anthropogenic forcing will not only lead to slow economic growth and climate warming, but
42 also likely result in environmental pollution issues.

43 **1. Introduction**

44 Tropospheric ozone (O₃), one major air pollutant, is formed in photochemical reactions of
45 nitrogen oxides (NO_x) and volatile organic compounds (VOCs) when exposed to sunlight
46 (Finlayson-Pitts and Pitts, 1997; Silman, 1999). Enhanced O₃ pollution harms ecosystems and
47 human health (Fleming et al., 2018; Maji et al., 2019) by reducing crop yields (Ainsworth et
48 al., 2012; Mills et al., 2018) and aggravating cardiopulmonary disease (Ebi and McGregor,
49 2008; Liu et al. 2018). In recent years, near-surface ozone concentrations in many regions of
50 China have been increasing considerably (Verstraeten et al., 2015; Cheng et al., 2019; Zhang
51 et al., 2020, Li et al., 2019; Lu et al., 2018; Silver et al., 2018; Yin et al., 2019, Lu et al., 2020).
52 Lu et al. (2020) revealed that the daily maximum of 8-h average O₃ concentration (MDA8-O₃)
53 in China increased by 2.4 ppb per year (5.0% relative to the average) during April–September
54 over 2013–2019.

55 In addition to emissions, O₃ concentrations are influenced by meteorological factors such
56 as temperature, relative humidity, solar radiation, and winds (Mott et al., 2005; Fu and Tian,
57 2019; Gong and Liao, 2019; Li et al., 2019, 2020; Le et al., 2020; Zhao et al., 2020). Typically,
58 strong solar radiation, high surface air temperatures, and low relative humidity are conducive
59 to photochemical production of O₃, causing a raise of O₃ concentration (Peterson and Flowers,
60 1977; Xu, et al., 2011; Coates et al., 2016; Li et al., 2020; Dang et al., 2021). Wind speed is
61 negatively correlated with surface O₃ because low wind speed facilitates the accumulation of
62 O₃ upon production (Zhang et al., 2015; Wang et al., 2017; Liu and Wang, 2020). Han et al.
63 (2020) explored the impacts of various meteorological factors on the daily variation of summer
64 surface O₃ in eastern China based on a multiple linear regression method and suggested that

65 relative humidity is the primary factor affecting O₃ concentration in central and south parts of
66 eastern China, while temperature is the most important factor governing O₃ concentration in
67 north of eastern China. Gong and Liao (2019) reported that the meteorological characteristics
68 of O₃ pollution events in North China during 2014–2017 were the high daily maximum
69 temperature, low relative humidity, abnormal southerly winds and high pressure at 500 hPa.
70 These findings emphasize that meteorological factors play a crucial role in regulating O₃
71 pollution in China.

72 Atmospheric circulation patterns affect O₃ concentrations over China through changing
73 meteorological factors (Yang et al, 2014, 2022; Zhao and Wang, 2017; Shu et al., 2019; Dong
74 et al., 2020; Zhou et al., 2022). Zhao and Wang (2017) examined the influence of the Western
75 Pacific Subtropical high (WPSH) on O₃ over eastern China based on observations and
76 reanalysis data from 2014 to 2016. They found that stronger WPSH enhanced the moisture
77 transport to southern China, which was detrimental to the photochemical reaction of O₃,
78 leading to a decrease in surface O₃ concentration in southern China, whereas O₃ concentrations
79 in northern China increased under the stronger WPSH related to the dry and hot conditions
80 favoring O₃ production. On the basis of observational O₃ data and ERA5 reanalysis data during
81 2014–2018, Dong et al. (2019) analyzed the impact of synoptic patterns on summertime O₃
82 pollution in the North China Plain and revealed that the most severe O₃ pollution weather
83 pattern is associated with anomalous southwesterly winds, which carry dry, warm air from
84 inland southern China to the North China Plain and favor the chemical production of O₃. Zhou
85 et al. (2022) explored the impacts of Asian summer monsoon on the interannual variation of
86 O₃ concentrations based on surface measurements and GEOS-Chem model simulations. They

87 showed that the East Asian summer monsoon strength was positively correlated with O₃
88 concentration in south-central China and South Asian summer monsoon has complex effects
89 on O₃ pollution in China, mainly through changing transboundary transport related to large-
90 scale circulations.

91 As mentioned above, many previous studies have examined the meteorological
92 characteristics of O₃ pollution in China. However, they focused on O₃ pollution over limited
93 regions in China in each study (e.g., the North China Plain, southern China). These studies only
94 examined the meteorological characteristics of O₃ pollution in a short time period due to the
95 lack of observational data and did not consider the historical and future trends of these
96 meteorological factors. In this study, the meteorological characteristics conducive to the most
97 severe O₃ pollution in several polluted areas of China, including the North China Plain (NCP),
98 Yangtze River Delta (YRD), Sichuan Basin (SCB), and Pearl River Delta (PRD), are
99 respectively investigated based on the observed surface O₃ concentrations, reanalysis data, and
100 GEOS-Chem model simulations. Besides, the contributions from various chemical and
101 physical processes inducing regional O₃ pollution are quantified using an integrated process
102 rate (IPR) analysis method. The historical changes in these meteorological factors favoring the
103 most severe O₃ pollution over 1980–2019 are provided. Moreover, variations in future
104 meteorological patterns during 2021–2100 leading to severe O₃ pollution in China are
105 presented under the sustainable and high forcing scenarios according to the multi-model data
106 from the Coupled Model Intercomparison Project Phase 6 (CMIP6).

107 **2. Methods**

108 **2.1 Surface ozone observations and meteorological reanalysis**

109 Hourly surface O₃ concentrations are obtained from the Ministry of Ecology and
110 Environment (MEE) of China. The observational network was established in 2013 with 450
111 monitoring sites and increased to 1,500 monitoring sites by 2019, covering about 360 cities in
112 China. MDA8-O₃ are calculated based on hourly O₃ concentrations from April-September
113 during 2013 to 2020. In this study, O₃ pollution days are defined as the days when MDA8-O₃
114 exceeds 160 µg m⁻³ according to the China National Ambient Air Quality Standard (GB3095-
115 2012).

116 The meteorological fields are taken from the European Centre for Medium-Range
117 Weather Forecasts (ECMWF) ERA5 monthly reanalysis dataset during 1980–2020, with a
118 horizontal resolution of 0.25° × 0.25°. To explore the meteorological characteristics that are
119 conducive to O₃ pollution, sea level pressure (SLP), geopotential height (GPH) at 500 hPa,
120 wind fields at 850 hPa and 500 hPa, temperature at 2m (T2m) and surface relative humidity
121 (RH) are adopted, which can have significant impacts on O₃ variations in China (Jiang et al.,
122 2020; Dong et al., 2020; Le et al., 2020).

123 **2.2 GEOS-Chem model simulations**

124 O₃ concentrations and the related chemical and physical processes causing O₃ variations
125 over 1981–2020 are simulated in the global atmospheric chemistry model GEOS-Chem
126 (version V12.9.3), driven by the Modern-Era Retrospective analysis for Research and
127 Application, Version 2 (MERRA-2). Simulations are performed on 47 vertical layers from
128 surface to 0.01 hPa, and a horizontal grid of 2° latitude × 2.5° longitude. GEOS-Chem model
129 incorporates a fully coupled O₃-NO_x-hydrocarbon-aerosol chemical mechanism (Pye et al.,
130 2009; Mao et al., 2013; Sherwen et al., 2016). Boundary-layer mixing uses a non-local scheme

131 (Lin and McElroy, 2010), and stratospheric O₃ chemistry employs the linearized O₃
132 parameterization (LINOZ) (McLinden et al., 2000).

133 Global anthropogenic emissions driving the simulations are from the Community
134 Emissions Data System (CEDS, Hoesly et al., 2018) and biomass burning emissions are from
135 the Global Fire Emissions Database, Edition 4 (GFED4, Van der Werf et al., 2017). VOCs
136 emissions from biogenic sources are provided offline by the Model of Emissions of Gases and
137 Aerosols from Nature version 2.1 (MEGAN V2.1, Guenther et al., 2012). Lightning and soil
138 emissions are specified in the model (Hudman et al., 2012; Ott et al., 2010). Anthropogenic
139 emissions in China are updated with the Multi-resolution Emission Inventory (MEIC), a
140 localized emission dataset for China. Anthropogenic, biomass burning, biogenic and other
141 natural emissions are kept at 2017 levels during the simulations, so as to eliminate the influence
142 of emission changes on the interannual variation and trends of O₃. Simulated O₃ distributions
143 with the same configuration in GEOS-Chem have been extensively evaluated in many studies,
144 and the model has been reported to capture O₃ concentrations well in China (e.g., Li et al.,
145 2019; Lu et al., 2019; Ni et al., 2018).

146 **2.3 CMIP6 multi-model simulations**

147 The multi-model simulations from historical and the Scenario Model Intercomparison
148 Project (ScenarioMIP) in CMIP6 are used to analyze the historical variations and future trends
149 of meteorological conditions conducive to the most severe O₃ pollution. Two different future
150 scenarios of the Shared Socioeconomic Path (SSPs) are applied, including the sustainable
151 scenario (SSP1-2.6) and the high forcing scenario (SSP5-8.5). Totally simulations from 13
152 models (ACCESS-CM2, ACCESS-ESM1-5, CAS-ESM2-0, CMCC-CM2-SR5, CMCC-ESM2,

153 FGOALS-f3-L, FGOALS-g3, GFDL-ESM4, INM-CM4-8, INM-CM5-0, IPSL-CM6A-LR,
154 MPI-ESM1-2-HR, MPI-ESM1-2-LR) are analyzed in this study.

155 **3. Results**

156 **3.1 Meteorological characteristics conducive to regional ozone pollution**

157 To investigate the relationship between meteorological conditions and regional O₃
158 pollution in China, the frequencies of O₃ pollution days from April to October during 2013–
159 2020 are calculated for Beijing, Shanghai, Chengdu and Guangzhou, representing the typical
160 four polluted regions in China (i.e., NCP, YRD, SCB and PRD) (Figure 1). Observational data
161 show the highest frequencies of O₃ pollution days in June 2018, July 2017 and September 2019
162 in Beijing, Shanghai and Guangzhou, with pollution days up to 22, 20 and 19 days per month,
163 respectively. The top three highest frequencies of O₃ pollution days in Chengdu are in July
164 2016, July 2015 and July 2018 (16, 15 and 15 days per month, respectively). Variations in O₃
165 concentration in the real world are driven by changes in both meteorological factors and
166 emissions. With fixed emissions, the positive anomalies of near-surface O₃ concentrations over
167 NCP, YRD and PRD during their most polluted months can also be reproduced by the GEOS-
168 Chem model (Figure 2), suggesting that the O₃ pollutions during the most polluted months over
169 NCP, YRD and PRD are likely attributable to the anomalies of meteorological conditions. In
170 the top three O₃ polluted months in Chengdu, only in July 2015 the higher concentrations than
171 the long-term averages can be captured by the simulations with fixed emissions. Therefore, in
172 this study, we focus on the meteorological characteristics in June 2018, July 2017, July 2015
173 and September 2019, that were conducive to the most severe O₃ pollution over NCP, YRD,
174 SCB and PRD, respectively.

175 When O₃ pollution was the most severe over NCP in June 2018, an anomalous high
176 pressure occurred at 500 hPa over NCP (Fig. 3b), relative to the 40-year climatological
177 averages from 1980 to 2019, leading to positive T2m anomalies near the surface (Fig. 3c).
178 Anomalous lows located over northeastern China and northwestern Pacific (Fig. 3a) and the
179 associated anomalous northerly winds prevent the moisture moving from the ocean to NCP,
180 causing negative RH anomalies over NCP (Fig. 3d). The meteorological conditions with the
181 high T2m and low RH are favorable for the photochemical production of O₃. When the most
182 severe O₃ pollution occurred in July 2017, YRD was dominated by anomalous high pressure
183 in the lower and middle troposphere (Figs. 4a and 4b). Under the control of high pressure, the
184 meteorological conditions (e.g., high T2m and low RH) enhance the photochemical production
185 of O₃ (Figs. 4c and 4d). In the O₃ pollution event of SCB in July 2015, the negative T2m
186 anomaly is not conducive to the O₃ production (Fig. 5c), although the RH was low (Fig. 5d).
187 Meanwhile, the anomalous low over eastern China and northwestern Pacific in the middle
188 troposphere favors regional O₃ transport from the polluted source region over eastern China to
189 SCB (Fig. 5b) and the anomalous high over central-western China is conducive to the vertical
190 transport of upper tropospheric O₃ down to the lower troposphere (Fig. 5a). For the PRD in
191 September 2019, the anomalous high covering almost the entire China along with the
192 anomalous low over East China Sea generates northerly wind anomalies in the lower
193 troposphere over eastern China, which tend to transport polluted air from northern China and
194 weaken the inflow of oceanic clean air (Fig. 6). The temperature increase is much more
195 significant in the upwind regions as compared to PRD, suggesting that the strong regional
196 transport could be the primary reason causing this severe O₃ pollution event of PRD.

197 **3.2 Physical and chemical mechanisms leading to regional ozone pollution**

198 To further explore the mechanisms of meteorological changes leading to the severe O₃
199 pollution over the four typical polluted regions in China, contributions of individual chemical
200 and physical processes to O₃ variations are quantified based on the IPR analysis from GEOS-
201 Chem simulations and summarized in Table 1.

202 Consistent with the meteorological anomalies analyzed above, high temperature and low
203 RH meteorological conditions in NCP are conducive to the photochemical production of O₃.
204 During the polluted month over NCP, the chemical production of tropospheric O₃ is higher than
205 the long-term average by 2.36 Gg day⁻¹, while the horizontal transport also contributes to the
206 increase in O₃ mass by 1.58 Gg day⁻¹ (Table 1). Due to the enhanced northwesterly winds, the
207 import of O₃ mass from the north and west of NCP was increased by 1.80 and 0.62 Tg,
208 respectively (Table 2). In YRD, the chemical production (2.38 Gg day⁻¹) is also the dominant
209 process that drives the O₃ concentration increase during the most severe polluted month,
210 associated with the warm and dry conditions. Therefore, the anomalous chemical production
211 is the major process that induced O₃ pollution in NCP and YRD during the most severe polluted
212 months.

213 Different from NCP and YRD, horizontal transport is the main process that caused O₃
214 pollution in SCB and PRD during the most severe months. It contributes to the rate of increase
215 in O₃ mass by 5.10 and 6.67 Gg day⁻¹, respectively, over SCB and PRD, while other processes
216 tend to decrease the O₃ mass (Table 1). Due to the anomalous northerly winds over SCB, more
217 O₃ is transported into SCB from north (by 4.02 Tg), and the anomalous northeasterly winds
218 enhance the O₃ transport from the north and east of PRD by 1.97 and 1.09 Tg, respectively,

219 leading to the increase in O₃ concentrations over SCB and PRD during the most severe months
220 relative to the climatological averages (Table 2). Note that, the chemical production of
221 tropospheric O₃ decreased in SCB and PRD during the most severe months. It could have been
222 biased by the relatively coarse model resolution in this study (2° latitude × 2.5° longitude),
223 since that the SCB and PRD for calculating the chemical and physical processes only cover
224 limited grid boxes. Further studies should be performed using a model with finer resolution or
225 a nested simulation method.

226 **3.3 Historical and future changes in the meteorological conditions**

227 O₃ pollution has deteriorated in China during recent decades, which could be related to
228 the changes in meteorological conditions. Time series of T2m and RH anomalies in the polluted
229 months during the 1980–2019 and frequencies of high T2m and low RH months during 1980–
230 1999 and 2000–2019 over the four polluted regions in China based on ERA5 reanalysis data
231 are shown in Figure 7. Due to climate change, both the high temperature and low RH conditions
232 in NCP, YRD, SCB and PRD all increased during the past four decades (2000-2019 versus
233 1980-1999). Based on the analysis showing that chemical production is the dominant process
234 of the most severe O₃ pollution in NCP and YRD, the increases in the frequency of high
235 temperature and low RH indicate that severe O₃ pollution in both NCP and YRD has become
236 more frequent under the historical climate change. In SCB and PRD, the most severe O₃
237 pollution is more related to changes in regional transport. Similar to the analyzing method used
238 in previous studies (Li et al., 2018; Yang et al., 2021), the SLP and 500 hPa GPH over East
239 Asia and Western Pacific in the same month of each year similar to those during the most severe
240 months in both SCB and PRD have increased (2000-2019 versus 1980-1999) (Figure 8),

241 together with the more frequent hot and dry conditions (Figure 7), leading to the increases in
242 severe O₃ pollution in SCB and PRD during 1980–2019.

243 Many studies have reported that future climate change will have significant influences
244 on O₃ pollution in China through changing meteorological factors (e.g., Li et al., 2023; Wang
245 et al., 2022). Here, the frequencies of extreme months with high T2m and low RH and the
246 frequencies of extreme months with SLP and 500 hPa GPH that have moderate to high
247 correlation to those in the most polluted months in the four regions of China, under the
248 sustainable (SSP1-2.6) and high forcing (SSP5-8.5) scenarios during 2021–2100 from CMIP6
249 multi-model results, are presented in Figures 9 and 10, respectively. Unlike the historical
250 changes in the meteorological conditions that caused the severe O₃ pollution through chemical
251 production and regional transport, future variations in meteorological conditions conducive to
252 the severe O₃ pollution are more related to the global warming process that enhances the O₃
253 production in China. The frequencies of months with anomalous high temperature show
254 obvious upward trends in both SSP1-2.6 and SSP5-8.5 scenarios over the four regions, and the
255 increasing trends in SSP5-8.5 are much more significant than in SSP1-2.6. Frequencies of low
256 RH months show downward trends in NCP, YRD and SCB, especially under SSP5-8.5, while
257 there is an upward trend in PRD. Note that the trends in frequencies of low RH months are
258 much less significant than in high temperature months. The frequencies of extreme months
259 with SLP and 500 hPa GPH that are similar to those in the most severe O₃ pollution months in
260 the four regions do not show significant trends in the SSPs. Hence, the future climate change
261 may aggregate O₃ pollution in China by enhancing the chemical production related to
262 temperature increases. The O₃ pollution exacerbation is projected to be less significant in the

263 sustainable scenario due to the moderate temperature increase than in the high forcing scenario,
264 suggesting that the sustainable scenario is the optimal path to retaining clean air in China. High
265 anthropogenic radiative forcing will not only lead to slow economic growth and climate
266 warming, but also result in the environmental pollution.

267 **4. Conclusions and Discussions**

268 O₃ pollution harms ecosystems and human health. In recent years, near-surface O₃
269 concentrations in many regions of China have been increasing considerably. Base on
270 observational O₃ data, ERA5 reanalysis data and GEOS-Chem model simulations,
271 meteorological characteristics conducive to extreme O₃ pollution in different regions of China
272 are investigated in this study. Contributions from various chemical and physical processes
273 inducing O₃ pollution are quantified using the IPR analysis method. Furthermore, historical
274 changes and future trends of meteorological conditions leading to severe O₃ pollution in China
275 are explored based on the meteorological reanalysis and CMIP6 multi-model future predictions,
276 which is of great implication for the mitigation and prevention of O₃ pollution over China.

277 In this study, June 2018, July 2017, July 2015 and September 2019 are identified as the
278 most severe O₃ pollution months influenced by meteorological factors over NCP, YRD, SCB
279 and PRD, respectively. Severe O₃ pollution in June 2018 over NCP and in July 2017 over YRD
280 is mainly due to enhanced chemical production related to hot and dry conditions. The chemical
281 production of O₃ in the most severe months over NCP and YRD are 2.36 Gg day⁻¹ and 2.38 Gg
282 day⁻¹, respectively, higher than the climatological averages. Different from NCP and YRD,
283 regional transport is the main process leading to the high O₃ concentration in SCB and PRD
284 during the respective severely polluted months, which contributes to the rate of increase in O₃

285 mass by 5.10 and 6.67 Gg day⁻¹, respectively, over SCB and PRD. During the most severe
286 months, related to large-scale circulation patterns, anomalous northerly winds transport more
287 O₃ into SCB from north, and anomalous northeasterly winds enhance the O₃ transport from the
288 north and east into PRD.

289 Over the last four decades (2000-2019 versus 1980-1999), the frequencies of high
290 temperature and low RH increased, indicating that O₃ pollution in both NCP and YRD has
291 become more frequent under the historical climate change. In SCB and PRD, the occurrence
292 of atmospheric circulation patterns similar to those during the most polluted months in both
293 SCB and PRD has increased, together with the more frequent hot and dry conditions, leading
294 to the increases in severe O₃ pollution in SCB and PRD during 1980–2019. In the future (by
295 2100), the frequencies of months with anomalous high temperature show obvious upward
296 trends in both sustainable (SSP1-2.6) and high forcing (SSP5-8.5) scenarios over the four
297 regions, and the increasing trends in SSP5-8.5 are much more significant than in SSP1-2.6.
298 This suggests that high anthropogenic radiative forcing will not only lead to slow economic
299 growth and climate warming, but also likely result in environmental pollution issues. The
300 sustainable scenario is the optimal path to retaining clean air in China.

301 There are some limitations and uncertainties in this work that can be further addressed in
302 future studies. For example, the model only captures the high O₃ concentrations in July 2015
303 in Chengdu among its top three polluted months. It is probably because the emissions are kept
304 at 2017 levels during the simulations. The high O₃ anomalies in July 2016 and July 2018 are
305 more likely influenced by the interannual changes in local precursor emissions in the
306 background of country-level increases in O₃ concentration in recent years. However, we also

307 can not rule out the possible inaccuracy in the model simulations to interpret severe O₃
308 pollution events in the SCB, which deserves further investigation with multi-model simulations.
309 In addition, this study focuses on the most extreme O₃ pollution in several polluted areas of
310 China. However, many other meteorological conditions can also cause O₃ pollution, although
311 they may not be as extreme as the cases analyzed in this study, which requires comprehensive
312 analysis for individual regions in future studies. Although the historical changes in the
313 meteorological patterns causing severe O₃ pollution are in accordance with the elevated O₃
314 levels in China in the recent decade, the quantitative analysis of meteorological impacts needs
315 full consideration of factors leading to O₃ pollution, including changes in anthropogenic and
316 natural emissions of its precursors, O₃ chemical regime, other meteorological factors conducive
317 to O₃ pollution, and stratosphere-troposphere exchange.

318

319 **References**

- 320 Ainsworth, E. A., Yendrek, C. R., Sitch, S., Collins, W. J., and Emberson, L. D.: The Effects of
321 Tropospheric Ozone on Net Primary Productivity and Implications for Climate Change,
322 *Annu. Rev. Plant Biol.*, 63, 637-661, [https://doi.org/10.1146/annurev-arplant-042110-](https://doi.org/10.1146/annurev-arplant-042110-103829)
323 103829, 2012.
- 324
- 325 Cheng, N., Li, R., Xu, C., Chen, Z., Chen, D., Meng, F., Cheng, B., Ma, Z., Zhuang, Y., He, B.,
326 and Gao, B.: Ground ozone variations at an urban and a rural station in Beijing from 2006
327 to 2017: trend, meteorological influences and formation regimes, *J. Clean. Prod.*, 235, 11–
328 20, <https://doi.org/10.1016/j.jclepro.2019.06.204>, 2019.
- 329
- 330 Coates, J., Mar, K. A., Ojha, N., and Butler, T. M.: The influence of temperature on ozone
331 production under varying NO_x conditions—a modelling study, *Atmos. Chem. Phys.*, 16,
332 11601-11615, <https://doi.org/10.5194/acp-16-11601-2016>, 2016.
- 333
- 334 Dang, R., Liao, H., and Fu, Y.: Quantifying the anthropogenic and meteorological influences
335 on summertime surface ozone in China over 2012-2017, *Sci. Total Environ.*, 754, 142394,
336 <https://doi.org/10.1016/j.scitotenv.2020.142394>, 2021.
- 337
- 338 Dong, Y., Li, J., Guo, J., Jiang, Z., Chu, Y., Chang, L., Yang, Y., and Liao, H.: The impact of
339 synoptic patterns on summertime ozone pollution in the North China Plain, *Sci. Total*
340 *Environ.*, 735, 139559, <https://doi.org/10.1016/j.scitotenv.2020.139559>, 2020.
- 341
- 342 Ebi, K. L. and McGregor, G.: Climate change, tropospheric O₃ and particulate matter, and
343 health impacts, *Environ. Health Perspect.*, 116, 1449-1455,
344 <https://doi.org/10.1289/ehp.11463>, 2008.
- 345
- 346 Finlayson-Pitts, B. J., and Pitts, J. N.: Tropospheric air pollution: Ozone, airborne toxics,
347 polycyclic aromatic hydrocarbons, and particles, *Science*, 276, 1045-1052,
348 <https://doi.org/10.1126/science.276.5315.1045>, 1997.
- 349
- 350 Fleming, Z. L., Doherty, R. M., Von Schneidemesser, E., Malley, C. S., Cooper, O. R., Pinto,
351 J. P., Colette, A., Xu, X. B., Simpson, D., Schultz, M. G., Lefohn, A. S., Hamad, S., Moolla,
352 R., Solberg, S., and Feng, Z. Z.: Tropospheric Ozone Assessment Report: Present-day
353 ozone distribution and trends relevant to human health, *Elementa-Sci. Anthropol.*, 6, 12,
354 <https://doi.org/10.1525/elementa.273>, 2018.
- 355
- 356 Fu, T.-M., and Tian, H.: Climate change penalty to ozone air quality: Review of current
357 understandings and knowledge gaps, *Curr. Pollution Rep.*, 5, 159–171,
358 <https://doi.org/10.1007/s40726-019-00115-6>, 2019.
- 359
- 360 Guenther, A. B., Jiang, X., Heald, C. L., Sakulyanontvittaya, T., Duhl, T., Emmons, L. K., and
361 Wang, X.: The Model of Emissions of Gases and Aerosols from Nature version 2.1
362 (MEGAN2.1): an extended and updated framework for modeling biogenic emissions,

363 Geosci. Model Dev., 5, 1471–1492, <https://doi.org/10.5194/gmd-5-1471-2012>, 2012.

364

365 Gong, C., and Liao, H.: A typical weather pattern for ozone pollution events in North China,
366 Atmos. Chem. Phys., 19, 13725–13740, <https://doi.org/10.5194/acp-19-13725-2019>,
367 2019.

368

369 Han, H., Liu, J., Shu, L., Wang, T. J., and Yuan, H.: Local and synoptic meteorological
370 influences on daily variability in summertime surface ozone in eastern China, Atmos.
371 Chem. Phys., 20, 203–222, <https://doi.org/10.5194/acp-20-203-2020>, 2020.

372

373 Hoesly, R. M., Smith, S. J., Feng, L., Klimont, Z., Janssens-Maenhout, G., Pitkanen, T., Seibert,
374 J. J., Vu, L., Andres, R. J., Bolt, R. M., Bond, T. C., Dawidowski, L., Kholod, N.,
375 Kurokawa, J. I., Li, M., Liu, L., Lu, Z., Moura, M. C. P., O'Rourke, P. R., and Zhang, Q.:
376 Historical (1750–2014) anthropogenic emissions of reactive gases and aerosols from the
377 Community Emissions Data System (CEDs), Geosci. Model Dev., 11, 369–408,
378 <https://doi.org/10.5194/gmd-11-369-2018>, 2018.

379

380 Hudman, R. C., Moore, N. E., Mebust, A. K., Martin, R. V., Russell, A. R., Valin, L. C., and
381 Cohen, R. C.: Steps towards a mechanistic model of global soil nitric oxide emissions:
382 implementation and space based-constraints, Atmos. Chem. Phys., 12, 7779–7795,
383 <https://doi.org/10.5194/acp-12-7779-2012>, 2012.

384

385 Jiang, Z., Li, J., Lu, X., Gong, C., Zhang, L., and Liao, H.: Impact of western Pacific subtropical
386 high on ozone pollution over eastern China, Atmos. Chem. Phys., 21, 2601–2613,
387 <https://doi.org/10.5194/acp-21-2601-2021>, 2021.

388

389 Le, T., Wang, Y., Liu, L., Yang, J., Yung, Y., Li, G., and Seinfeld, J. H.: Unexpected air pollution
390 with marked emission reductions during the COVID-19 outbreak in China, Science, 369,
391 702–706, <https://doi.org/10.1126/science.abb7431>, 2020.

392

393 Li, H., Yang, Y., Jin, J., Wang, H., Li, K., Wang, P., and Liao, H.: Climate-driven deterioration
394 of future ozone pollution in Asia predicted by machine learning with multi-source data,
395 Atmos. Chem. Phys., 23, 1131–1145, <https://doi.org/10.5194/acp-23-1131-2023>, 2023.

396

397 Li, K., Liao, H., Cai, W., and Yang, Y.: Attribution of anthropogenic influence on atmospheric
398 patterns conducive to recent most severe haze over eastern China, Geophys. Res. Lett.,
399 45, 2072–2081, <https://doi.org/10.1002/2017gl076570>, 2018.

400

401 Li, K., Jacob, D. J., Liao, H., Shen, L., Zhang, Q., and Bates, K. H.: Anthropogenic drivers of
402 2013–2017 trends in summer surface ozone in China, P. Natl. Acad. Sci. USA, 116, 422–
403 427, <https://doi.org/10.1073/pnas.1812168116>, 2019.

404

405 Li, K., Jacob, D. J., Shen, L., Lu, X., De Smedt, I., and Liao, H.: Increases in surface ozone
406 pollution in China from 2013 to 2019: anthropogenic and meteorological influences,

407 Atmos. Chem. Phys., 20, 11423–11433, <https://doi.org/10.5194/acp-20-11423-2020>, 2020.
408

409 Lin, J.-T., and McElroy, M. B.: Impacts of boundary layer mixing on pollutant vertical profiles
410 in the lower troposphere: Implications to satellite remote sensing, *Atmos. Environ.*, 44,
411 1726–1739, <https://doi.org/10.1016/j.atmosenv.2010.02.009>, 2010.
412

413 Liu, H., Liu, S., Xue, B., Lv, Z., Meng, Z., Yang, X., Xue, T., Yu, Q., and He, K.: Ground-level
414 ozone pollution and its health impacts in China, *Atmos. Environ.*, 173, 223–230,
415 <https://doi.org/10.1016/j.atmosenv.2017.11.014>, 2018.
416

417 Liu, Y., and Wang, T.: Worsening urban ozone pollution in China from 2013 to 2017–Part 1:
418 The complex and varying roles of meteorology, *Atmos. Chem. Phys.*, 20, 6305–6321,
419 <https://doi.org/10.5194/acp-20-6305-2020>, 2020.
420

421 Lu, X., Hong, J., Zhang, L., Cooper, O. R., Schultz, M. G., Xu, X., Wang, T., Gao, M., Zhao,
422 Y., and Zhang, Y.: Severe Surface Ozone Pollution in China: A Global Perspective,
423 *Environ. Sci. Technol. Lett.*, 5, 487–494, <https://doi.org/10.1021/acs.estlett.8b00366>,
424 2018.
425

426 Lu, X., Zhang, L., Chen, Y., Zhou, M., Zheng, B., Li, K., Liu, Y., Lin, J., Fu, T.-M., and Zhang,
427 Q.: Exploring 2016–2017 surface ozone pollution over China: source contributions and
428 meteorological influences, *Atmos. Chem. Phys.*, 19, 8339–8361,
429 <https://doi.org/10.5194/acp-19-8339-2019>, 2019.
430

431 Lu, X., Zhang, L., Wang, X., Gao, M., Li, K., Zhang, Y., Yue, X., and Zhang, Y.: Rapid increases
432 in warm-season surface ozone and resulting health impact over China since 2013, *Environ.*
433 *Sci. Technol. Lett.*, 7, 240–247, <https://doi.org/10.1021/acs.estlett.0c00171>, 2020.
434

435 Maji, K. J., Ye, W.-F., Arora, M., and Nagendra, S. M. S.: Ozone pollution in Chinese cities:
436 Assessment of seasonal variation, health effects and economic burden, *Environ. Pollut.*,
437 247, 792–801, <https://doi.org/10.1016/j.envpol.2019.01.049>, 2019.
438

439 Mao, J., Paulot, F., Jacob, D. J., Cohen, R. C., Crouse, J. D., Wennberg, P. O., Keller, C. A.,
440 Hudman, R. C., Barkley, M. P., and Horowitz, L. W.: Ozone and organic nitrates over the
441 eastern United States: Sensitivity to isoprene chemistry, *J. Geophys. Res. Atmos.*, 118,
442 11256–11268, <https://doi.org/10.1002/jgrd.50817>, 2013.
443

444 McLinden, C. A., Olsen, S. C., Hannegan, B., Wild, O., Prather, M. J., and Sundet, J.:
445 Stratospheric ozone in 3-D models: A simple chemistry and the cross-tropopause flux, *J.*
446 *Geophys. Res.*, 105, 14653–14665, <https://doi.org/10.1029/2000jd900124>, 2000.
447

448 Mills, G., Sharps, K., Simpson, D., Pleijel, H., Broberg, M., Uddling, J., Jaramillo, F., Davies,
449 W. J., Dentener, F., Van den Berg, M., Agrawal, M., Agrawal, S. B., Ainsworth, E. A.,
450 Buker, P., Emberson, L., Feng, Z., Harmens, H., Hayes, F., Kobayashi, K., Paoletti, E.,

451 and Van Dingenen, R.: Ozone pollution will compromise efforts to increase global wheat
452 production, *Glob. Chang. Biol.*, 24, 3560-3574, <https://doi.org/10.1111/gcb.14157>, 2018.

453

454 Mott, J. A., Mannino, D. M., Alverson, C. J., Kiyu, A., Hashim, J., Lee, T., Falter, K., Redd, S.
455 C.: Cardiorespiratory hospitalizations associated with smoke exposure during the 1997
456 southeast Asian forest fires, *Int. J. Hyg. Environ. Health.*, 208, 75–85,
457 <https://doi.org/10.1016/j.ijheh.2005.01.018>, 2005.

458

459 Ni, R., Lin, J., Yan, Y., and Lin, W.: Foreign and domestic contributions to springtime ozone
460 over China, *Atmos. Chem. Phys.*, 18, 11447–11469, [https://doi.org/10.5194/acp-18-](https://doi.org/10.5194/acp-18-11447-2018)
461 [11447-2018](https://doi.org/10.5194/acp-18-11447-2018), 2018.

462

463 Ott, L. E., Pickering, K. E., Stenchikov, G. L., Allen, D. J., DeCaria, A. J., Ridley, B., Lin, R.-
464 F., Lang, S., and Tao, W.-K.: Production of lightning NO_x and its vertical distribution
465 calculated from three-dimensional cloud-scale chemical transport model simulations, *J.*
466 *Geophys. Res.*, 115, D04301, <https://doi.org/10.1029/2009JD011880>, 2010.

467

468 Peterson, J. T., and Flowers, E. C.: Interactions between air pollution and solar radiation, *Sol.*
469 *Energy*, 19, 23–32, [https://doi.org/10.1016/0038-092X\(77\)90085-8](https://doi.org/10.1016/0038-092X(77)90085-8), 1977.

470

471 Pye, H. O., Liao, H., Wu, S., Mickley, L. J., Jacob, D. J., Henze, D. K., and Seinfeld, J. H.:
472 Effect of changes in climate and emissions on future sulfate-nitrate-ammonium aerosol
473 levels in the United States, *J. Geophys. Res.*, 114, D01205,
474 <https://doi.org/10.1029/2008JD010701>, 2009.

475

476 Sherwen, T., Schmidt, J. A., Evans, M. J., Carpenter, L. J., Großmann, K., Eastham, S. D.,
477 Jacob, D. J., Dix, B., Koenig, T. K., Sinreich, R., Ortega, I., Volkamer, R., Saiz-Lopez, A.,
478 Prados-Roman, C., Mahajan, A. S., and Ordóñez, C.: Global impacts of tropospheric
479 halogens (Cl, Br, I) on oxidants and composition in GEOS-Chem, *Atmos. Chem. Phys.*,
480 16, 12239–12271, <https://doi.org/10.5194/acp-16-12239-2016>, 2016.

481

482 Shu, L., Wang, T., Han, H., Xie, M., Chen, P., Li, M., and Wu, H.: Summertime ozone pollution
483 in the Yangtze River Delta of eastern China during 2013–2017: synoptic impacts and
484 source apportionment, *Environ. Pollut.*, 257, 113631,
485 <https://doi.org/10.1016/j.envpol.2019.113631>, 2020

486

487 Sillman, S.: The relation between ozone, NO_x and hydrocarbons in urban and polluted rural
488 environments, *Atmos. Environ.*, 33, 1821-1845, [https://doi.org/10.1016/s1352-](https://doi.org/10.1016/s1352-2310(98)00345-8)
489 [2310\(98\)00345-8](https://doi.org/10.1016/s1352-2310(98)00345-8), 1999.

490

491 Silver, B., Reddington, C. L., Arnold, S. R., and Spracklen, D. V.: Substantial changes in air
492 pollution across China during 2015–2017, *Environ. Res. Lett.*, 13, 114012,
493 <https://doi.org/10.1088/1748-9326/aae718>, 2018.

494

495 Sekiya, T., and Sudo, K.: Roles of transport and chemistry processes in global ozone change
496 on interannual and multidecadal time scales, *J. Geophys. Res. Atmos.*, 119, 4903–4921,
497 <https://doi.org/10.1002/2013JD020838>, 2014.
498

499 van der Werf, G. R., Randerson, J. T., Giglio, L., van Leeuwen, T. T., Chen, Y., Rogers, B. M.,
500 Mu, M., van Marle, M. J. E., Morton, D. C., Collatz, G. J., Yokelson, R. J., and Kasibhatla,
501 P. S.: Global fire emissions estimates during 1997–2016, *Earth Syst. Sci. Data*, 9, 697–
502 720, <https://doi.org/10.5194/essd-9-697-2017>, 2017.
503

504 Verstraeten, W. W., Neu, J. L., Williams, J. E., Bowman, K. W., Worden, J. R., and Boersma,
505 K. F.: Rapid increases in tropospheric ozone production and export from China, *Nat.*
506 *Geosci.*, 8, 690–695, <https://doi.org/10.1038/ngeo2493>, 2015.
507

508 Wang, P., Yang, Y., Li, H., Chen, L., Dang, R., Xue, D., Li, B., Tang, J., Leung, L. R., and Liao,
509 H.: North China Plain as a hot spot of ozone pollution exacerbated by extreme high
510 temperatures, *Atmos. Chem. Phys.*, 22, 4705–4719, [https://doi.org/10.5194/acp-22-4705-](https://doi.org/10.5194/acp-22-4705-2022)
511 [2022](https://doi.org/10.5194/acp-22-4705-2022), 2022.
512

513 Wang, T., Xue, L., Brimblecombe, P., Lam, Y. F., Li, L., and Zhang, L.: Ozone pollution in
514 China: A review of concentrations, meteorological influences, chemical precursors, and
515 effects, *Sci. Total Environ.*, 575, 1582–1596,
516 <https://doi.org/10.1016/j.scitotenv.2016.10.081>, 2017.
517

518 Xu, J., Ma, J. Z., Zhang, X. L., Xu, X. B., Xu, X. F., Lin, W. L., Wang, Y., Meng, W., and Ma,
519 Z. Q.: Measurements of ozone and its precursors in Beijing during summertime: impact
520 of urban plumes on ozone pollution in downwind rural areas, *Atmos. Chem. Phys.*, 11,
521 12241–12252, <https://doi.org/10.5194/acp-11-12241-2011>, 2011.
522

523 Yang, Y., Liao, H., and Li, J.: Impacts of the East Asian summer monsoon on interannual
524 variations of summertime surface-layer ozone concentrations over China, *Atmos. Chem.*
525 *Phys.*, 14, 6867–6880, <http://doi:10.5194/acp-14-6867-2014>, 2014.
526

527 Yang, Y., Zhou, Y., Li, K., Wang, H., Ren, L., Zeng, L., Li, H., Wang, P., Li, B., and Liao, H.:
528 Atmospheric circulation patterns conducive to severe haze in eastern China have shifted
529 under climate change, *Geophys. Res. Lett.*, 48, e2021GL095011,
530 <https://doi.org/10.1029/2021GL095011>, 2021.
531

532 Yang, Y., Li, M., Wang, H., Li, H., Wang, P., Li, K., Gao, M., and Liao, H.: ENSO modulation
533 of summertime tropospheric ozone over China, *Environ. Res. Lett.*, 17, 034020,
534 <https://doi.org/10.1088/1748-9326/ac54cd>, 2022.
535

536 Yin, Z., Cao, B., and Wang, H.: Dominant patterns of summer ozone pollution in eastern China
537 and associated atmospheric circulations, *Atmos. Chem. Phys.*, 19, 13933–13943,
538 <https://doi.org/10.5194/acp-19-13933-2019>, 2019.

539
540
541
542
543
544
545
546
547
548
549
550
551
552
553
554
555
556
557
558
559
560
561

Zhang, X., Zhao, L., Cheng, M., Wu, X., and Chen, D.: Urban ozone sink inferred from surface measurements in China, *J. Clean. Prod.*, 253, 119881, <https://doi.org/10.1016/j.jclepro.2019.119881>, 2020.

Zhang, H., Wang, Y., Hu, J., Ying, Q., and Hu, X.-M.: Relationships between meteorological parameters and criteria air pollutants in three megacities in China, *Environ. Res.*, 140, 242–254, <https://doi.org/10.1016/j.envres.2015.04.004>, 2015.

Zhao, Y., Zhang, K., Xu, X., Shen, H., Zhu, X., Zhang, Y., Hu, Y., and Shen, G.: Substantial changes in nitrogen dioxide and ozone after excluding meteorological impacts during the COVID-19 outbreak in mainland China, *Environ. Sci. Technol. Lett.*, 7, 402–408, <https://doi.org/10.1021/acs.estlett.0c00304>, 2020.

Zhao, Z., and Wang, Y.: Influence of the West Pacific subtropical high on surface ozone daily variability in summertime over eastern China, *Atmos. Environ.*, 170, 197–204, <https://doi.org/10.1016/j.atmosenv.2017.09.024>, 2017.

Zhou, D., Ding, A., Mao, H., Fu, C., Wang, T., Chan, L. Y., Ding, K., Zhang, Y., Liu, J., and Lu, A.: Impacts of the East Asian monsoon on lower tropospheric ozone over coastal South China, *Environ. Res. Lett.*, 8, 044011, <https://doi.org/10.1088/1748-9326/8/4/044011>, 2013.

562 **Code and data availability.** The GEOS-Chem model is available at
563 <https://zenodo.org/record/3974569#.YTD81NMzagR> (last access: June 2023). O₃ observations
564 over China can be obtained at <https://quotsoft.net/air> (last access: June 2023). ERA5 reanalysis
565 data can be downloaded at [https://www.ecmwf.int/en/forecasts/datasets/reanalysis-](https://www.ecmwf.int/en/forecasts/datasets/reanalysis-datasets/era5)
566 [datasets/era5](https://www.ecmwf.int/en/forecasts/datasets/reanalysis-datasets/era5) (last access: June 2023). The multi-model simulations of the Coupled Model
567 Intercomparison Project Phase 6 (CMIP6) are from <https://esgf-node.llnl.gov/search/cmip6/>
568 (last access: June 2023).

569 **Author contribution.** YY designed the research; YY and YZ performed simulations and
570 analyzed the data. All authors including HW, LH, PW, and HL discussed the results and wrote
571 the paper.

572 **Competing interests.** At least one of the (co-)authors is a member of the editorial board of
573 Atmospheric Chemistry and Physics.

574 **Acknowledgments.** HW acknowledges the support by the U.S. Department of Energy (DOE),
575 Office of Science, Office of Biological and Environmental Research (BER), as part of the Earth
576 and Environmental System Modeling program. The Pacific Northwest National Laboratory
577 (PNNL) is operated for DOE by the Battelle Memorial Institute under contract DE-AC05-
578 76RLO1830.

579 **Financial support.** This study was supported by the National Natural Science Foundation of
580 China (grant 42293323), and the National Key Research and Development Program of China
581 (grant 2020YFA0607803), Jiangsu Science Fund for Distinguished Young Scholars (grant
582 BK20211541), Jiangsu Science Fund for Carbon Neutrality (grant BK20220031), and the
583 Graduate Research Innovation Project in Jiangsu province (KYCX23_1380).

584 **Table 1.** Anomalies in net rate of changes in tropospheric O₃ mass (Gg day⁻¹) over NCP (115°–
585 120°E, 38°–44°N), YRD (120°–125°E, 28°–32°N), SCB (102.5°–105°E, 30°–32°N) and PRD
586 (110°–115°E, 22°–26°N) due to physical and chemical processes in the most polluted months
587 (June 2018, July 2017, July 2015 and September 2019, respectively) relative to the same
588 months averaged during 1981–2019.

589

	Beijing	Shanghai	Chengdu	Guangzhou
Chemical reaction	2.36	2.38	-2.80	-1.52
Horizontal transport	1.58	-1.18	5.10	6.67
Diffusion and dry deposition	0.29	0.24	-0.73	-0.93

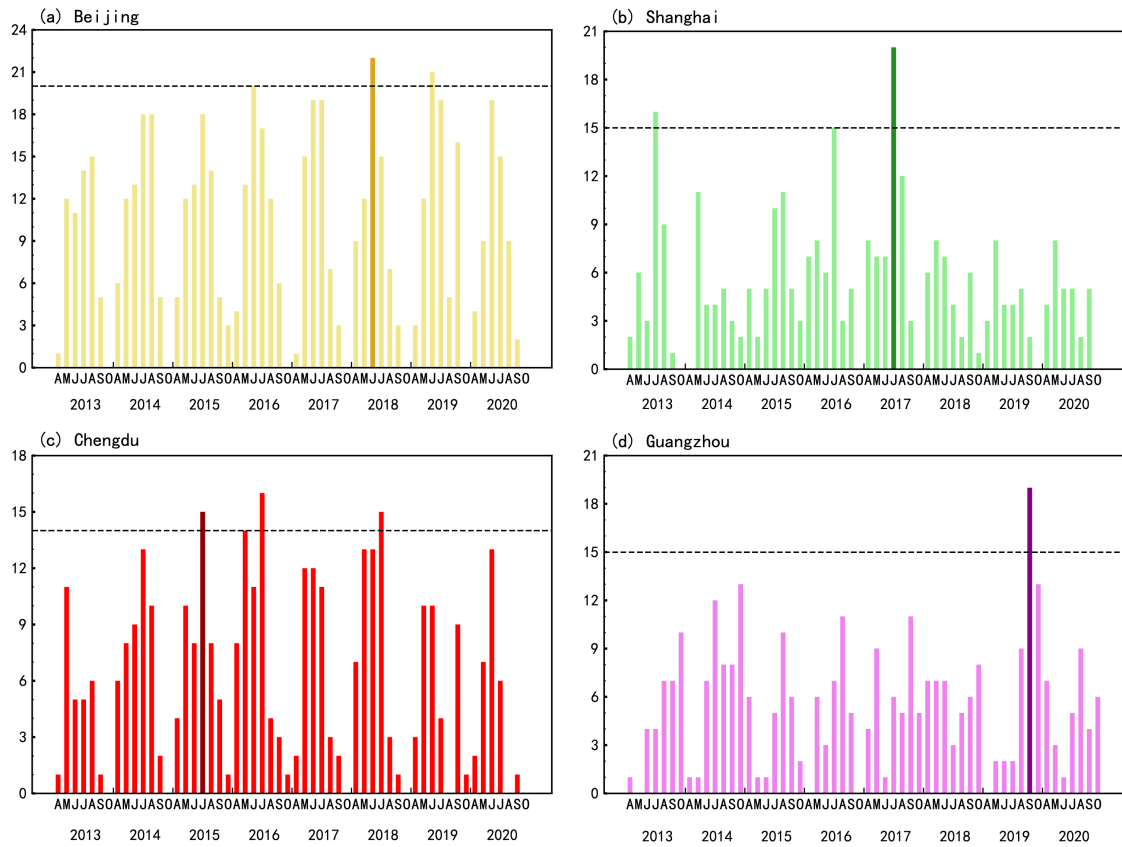
590

591

592 **Table 2.** Horizontal mass transport (Tg) of O₃ from the surface to 500 hPa over NCP (115°–
593 120°E, 38°–44°N), YRD (120°–125°E, 28°–32°N), SCB (102.5°–105°E, 30°–32°N) and PRD
594 (110°–115°E, 22°–26°N) areas in the severe polluted months (June 2018, July 2017, July 2015
595 and September 2019, respectively) and averaged over the same months of a year during 1981–
596 2019, as well as their differences. Positive values indicate incoming fluxes and negative values
597 indicate outgoing fluxes.
598

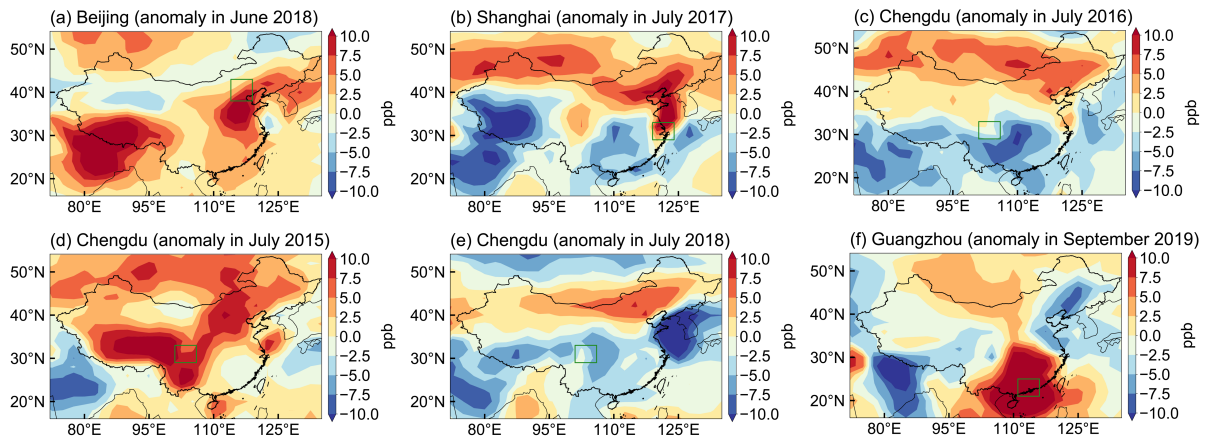
	Polluted month	Average	Anomalies
NCP			
North	4.43	2.62	1.80
South	-2.22	-1.42	-0.81
East	-12.30	-11.31	-0.99
West	11.83	11.20	0.62
YPD			
North	-4.13	-3.88	-0.25
South	3.58	3.20	0.37
East	-2.05	-3.90	1.85
West	2.03	4.04	-2.01
SCB			
North	4.15	0.13	4.02
South	-2.30	0.48	-2.78
East	-1.10	-1.15	0.05
West	1.73	1.84	-0.11
PRD			
North	2.70	0.72	1.97
South	-2.87	-0.90	-1.96
East	2.24	1.15	1.09
West	-2.32	-1.55	-0.76

599
600



601
602
603
604
605
606
607

Figure 1. Time series of frequencies of severe O₃ pollution days (defined by daily maximum of 8-h average ozone (MDA8-O₃) concentration greater than 160 µg m⁻³) in Beijing, Shanghai, Chengdu and Guangzhou (a–d) from April to October during 2013–2020. The dark-colored bars represent the most severe month (second most for Chengdu) that has the highest frequency of O₃ pollution days for the individual cities.



608

609

610

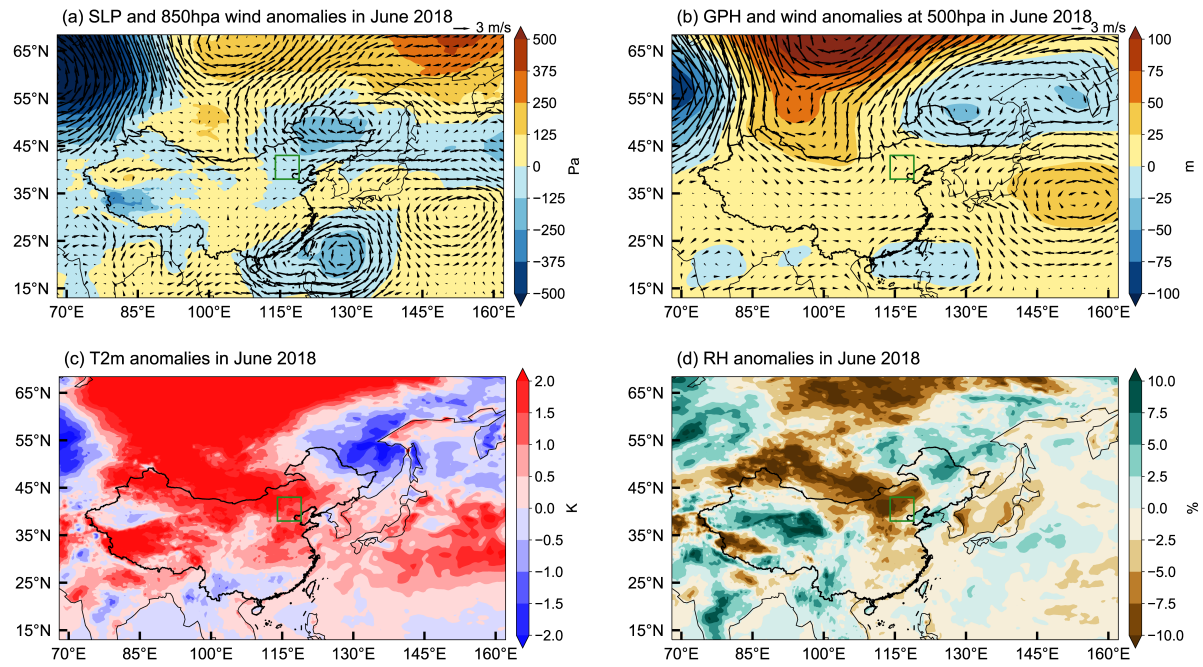
611

612

613

614

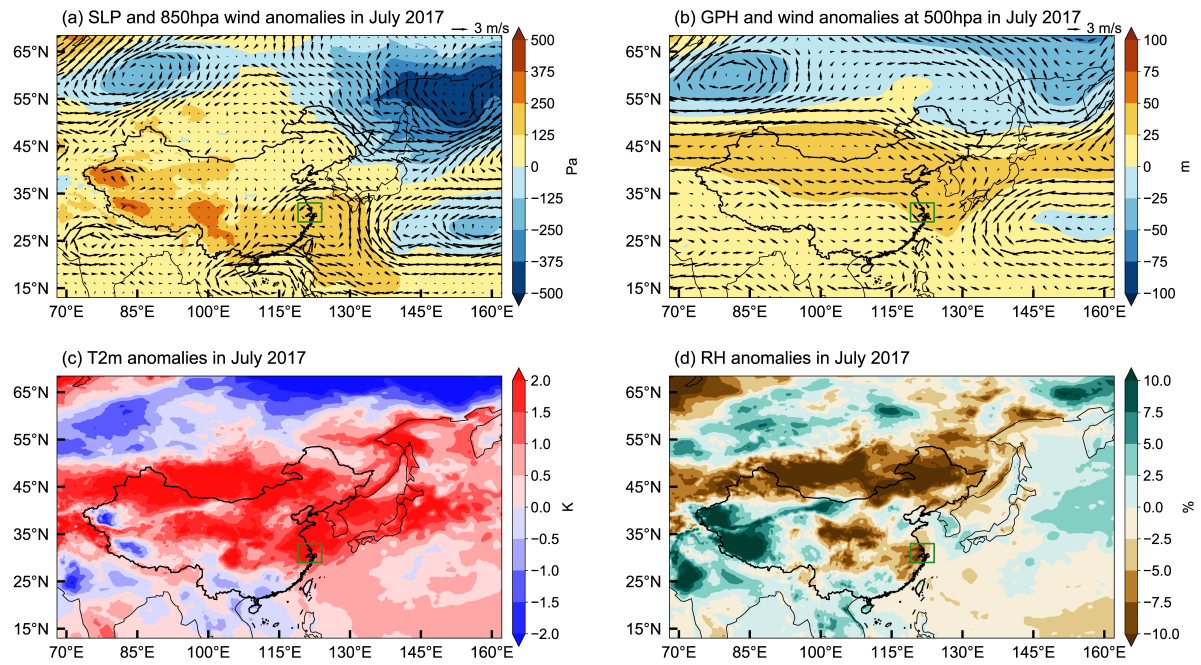
Figure 2. Spatial distribution of monthly O_3 concentration anomalies (part per billion, ppb) in June 2018 (a), July 2017 (b), July 2016 (c), July 2015 (d), July 2018 (e) and September 2019 (f) relative to 40-year (1980–2019) monthly average for June (a), July (b, c, d, e) and September (f), simulated in the GEOS-Chem model. The green boxes mark NCP (a), YRD (b), SCB (c, d, e) and PRD (f).



615

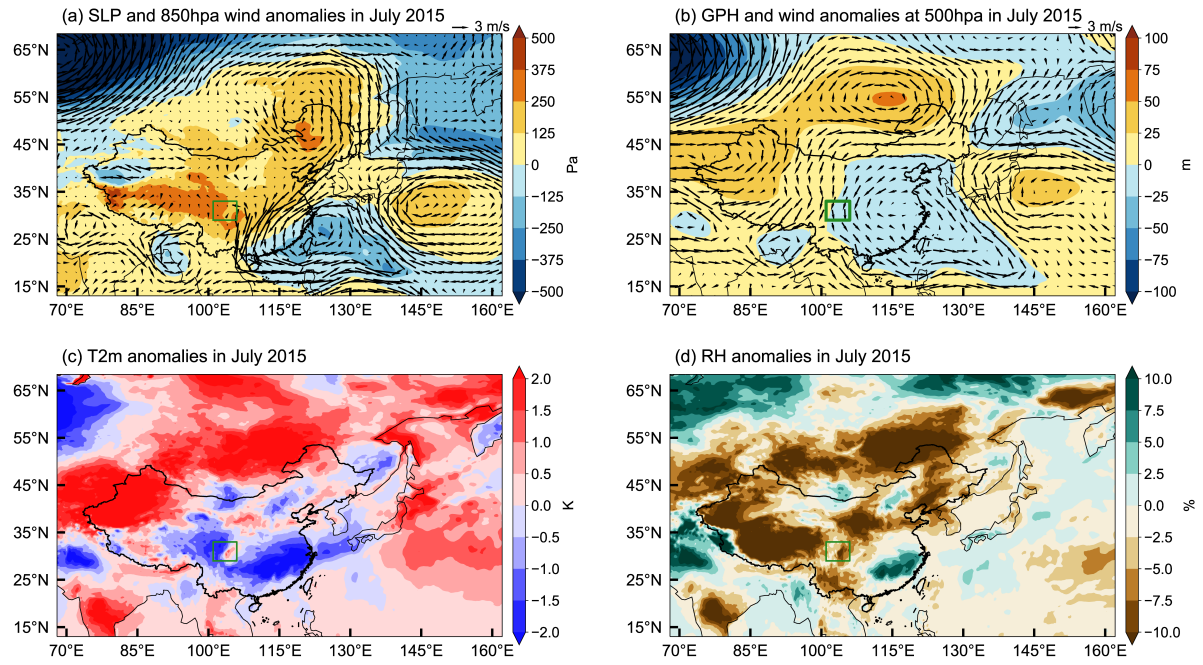
616 **Figure 3.** Anomalies in sea level pressure (SLP, Pa, shaded) and 850 hPa winds (m s^{-1} , vector)
 617 (a), geopotential height (GPH, m, shaded) and winds at 500 hPa (m s^{-1} , vector) (b), 2-meter air
 618 temperature (T2m, K) (c) and surface relative humidity (RH, %) (d) in June 2018 relative to
 619 the 40-year (1980–2019) monthly average for June. The green boxes mark NCP.

620



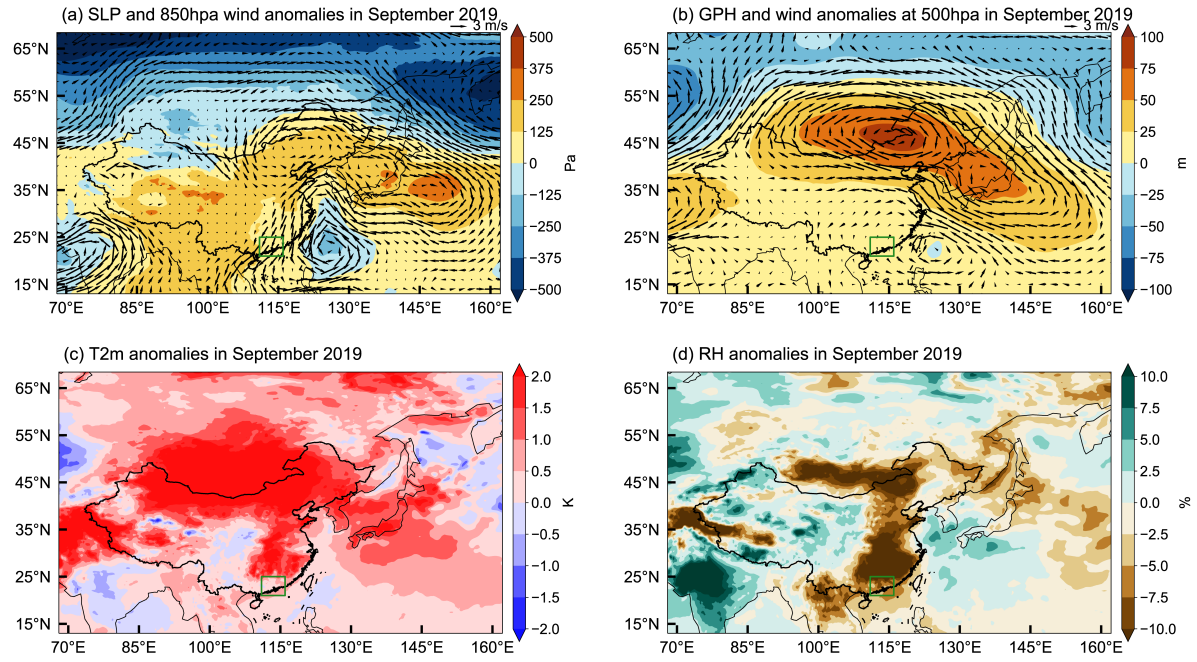
621
 622
 623
 624

Figure 4. Same as Figure 3 but for the monthly anomalies in July 2017. The green boxes mark YRD.



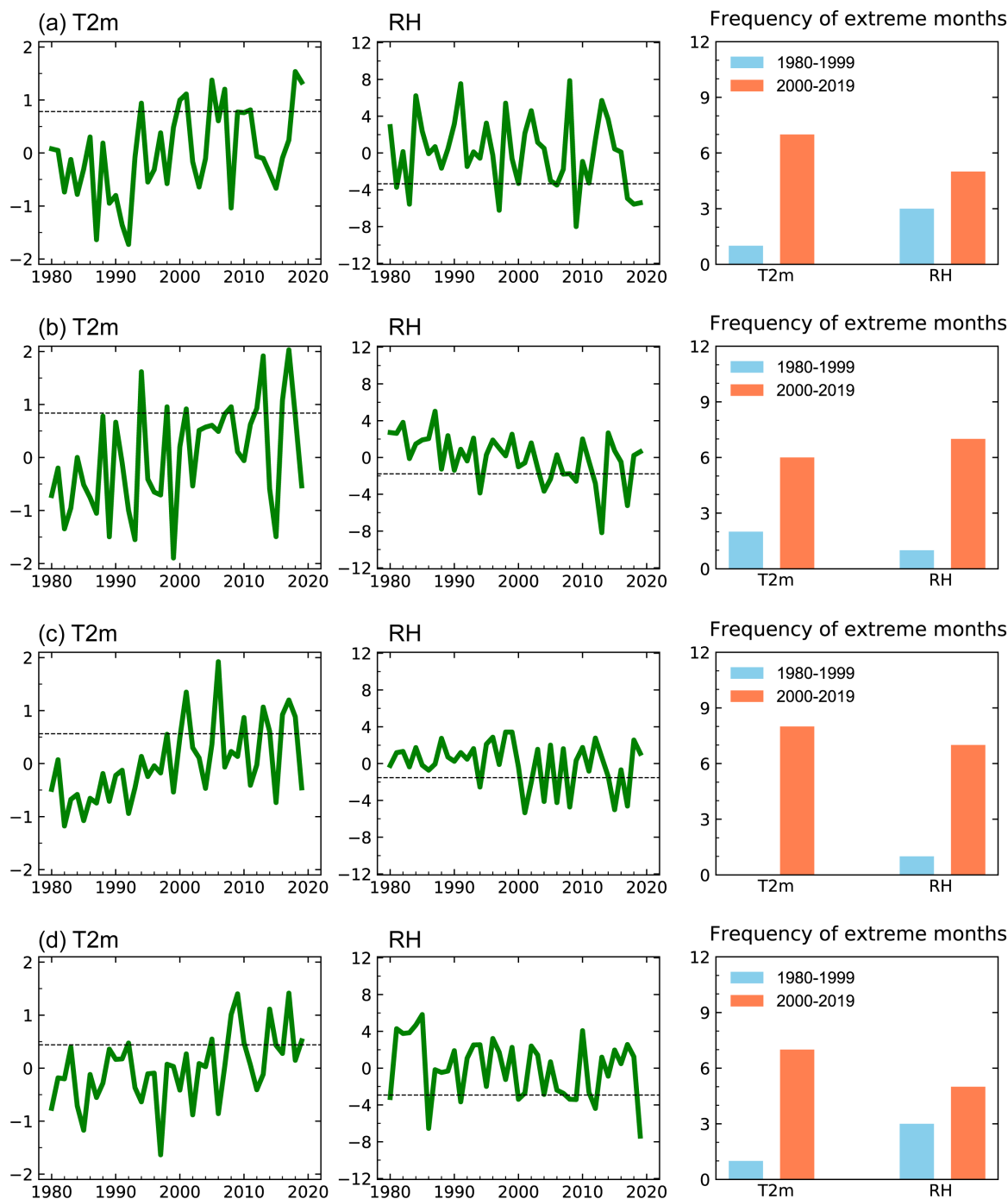
625
 626
 627
 628

Figure 5. Same as Figure 3 but for the monthly anomalies in July 2015. The green boxes mark SCB.



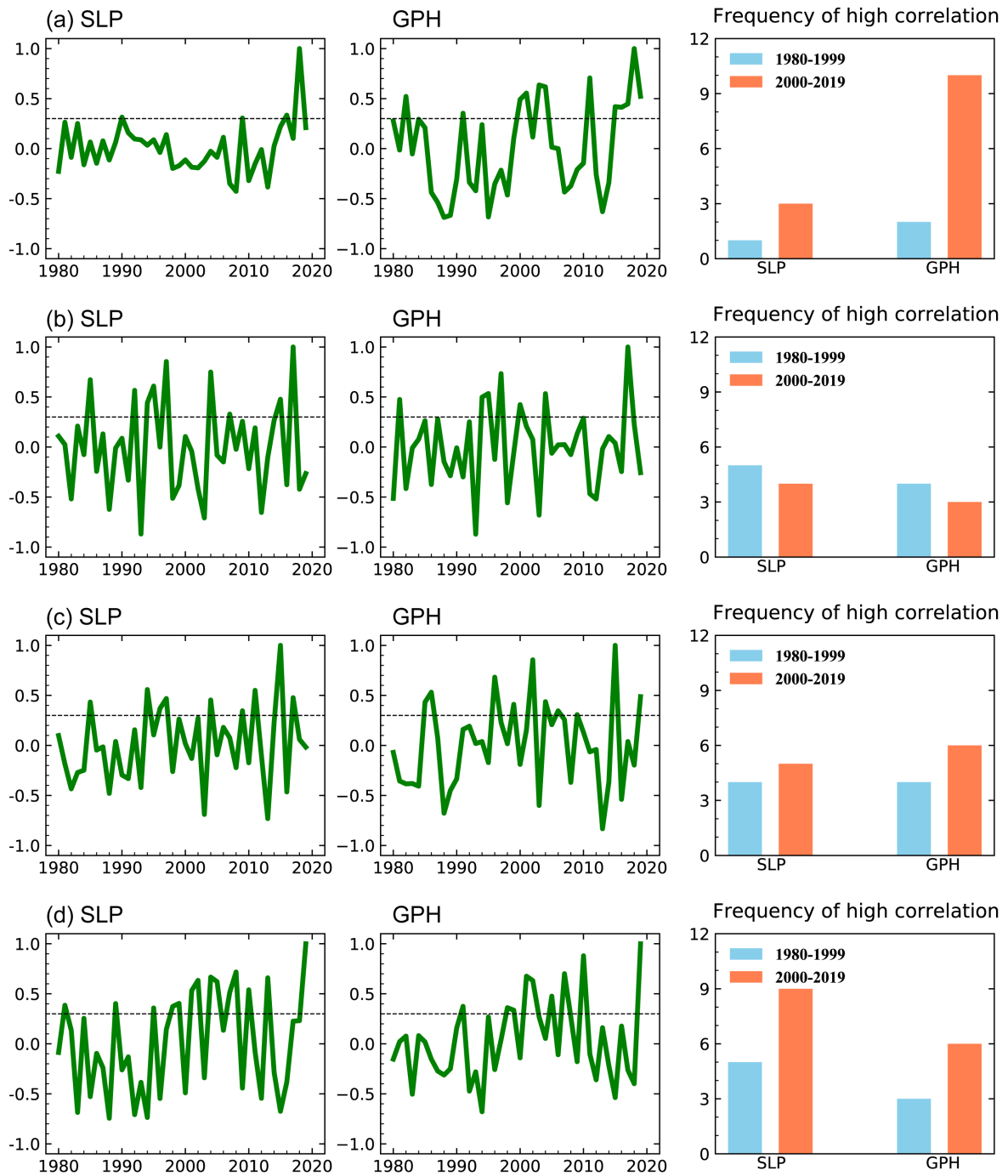
629

630 **Figure 6.** Same as Figure 3 but for the monthly anomalies in September 2019. The green boxes
 631 mark PRD.



632

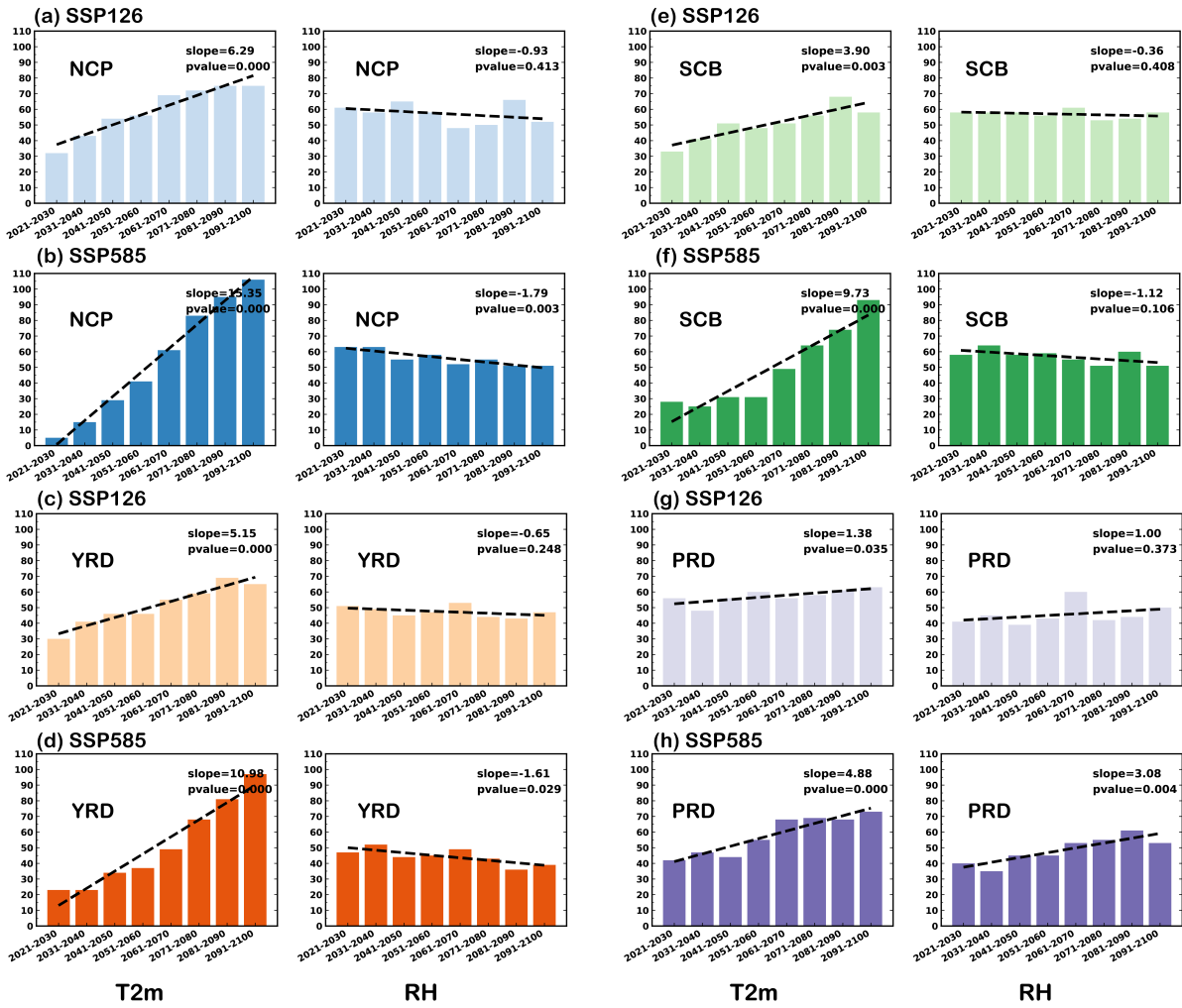
633 **Figure 7.** Time series of anomalies of T2m (K, left) and surface RH (%), middle) over (a) NCP
 634 (115°–120°E, 38°–44°N), (b) YRD (120°–125°E, 28°–32°N), (c) SCB (102.5°–105°E, 30°–
 635 32°N) and (d) PRD (110°–115°E, 22°–26°N) in the most polluted months during 1980–2019.
 636 The dotted lines mark the 80th percentile of the distributions for T2m and 20th percentile for
 637 RH. The bar charts (right) represent the frequency of T2m above the 80th percentile and RH
 638 anomalies below the 20th percentile during 1980–1999 (blue) and 2000–2019 (orange).



639

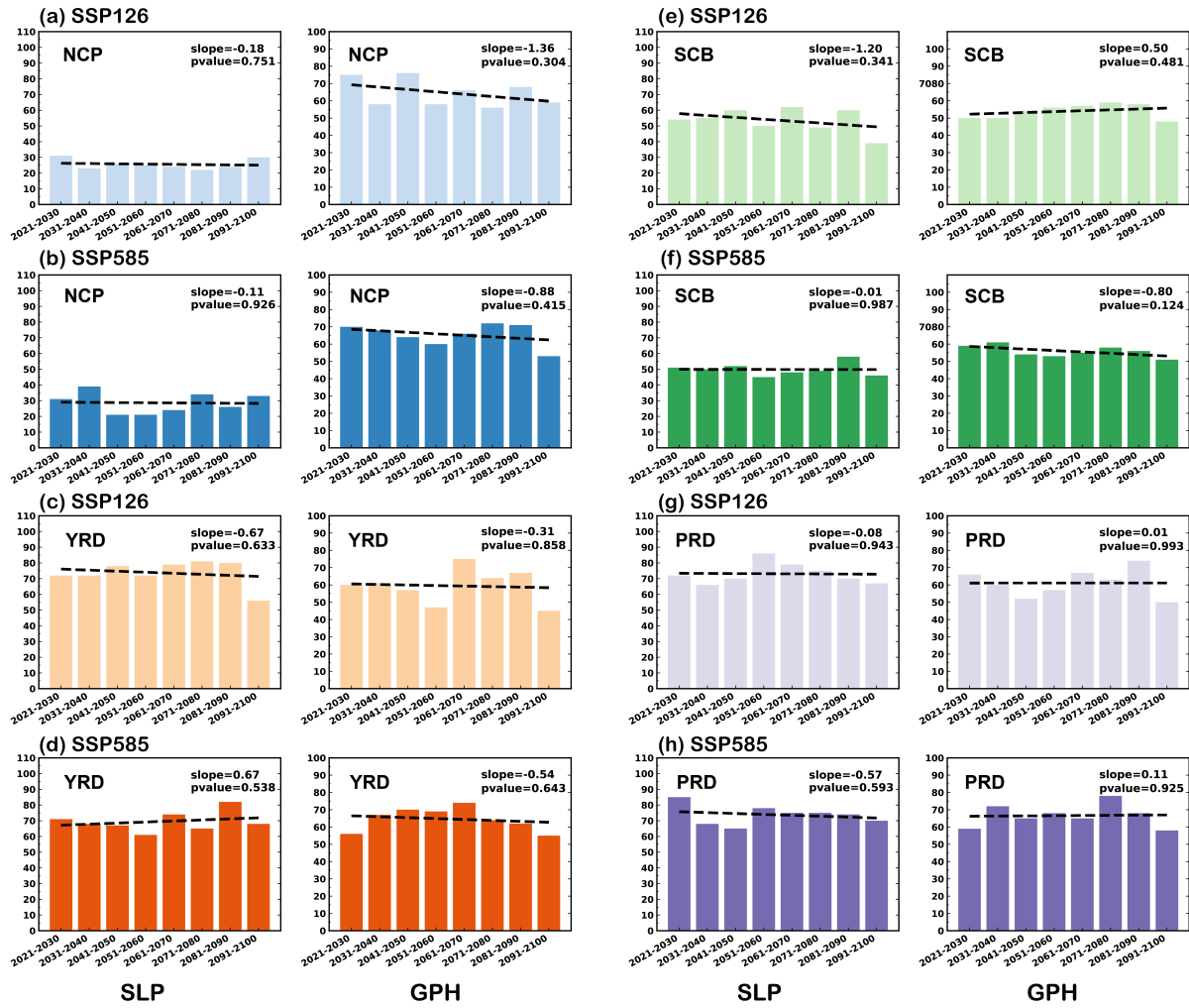
640 **Figure 8.** Time series of spatial correlation in SLP (left) and 500 hPa GPH (middle) anomalies
 641 over East Asia and Western Pacific (EAWP, 90°–160°E, 20°–60°N) in June 2018 (a), July 2017
 642 (b), July 2015 (c) and September 2019 (d) and those in the same targeted month of each year
 643 during 1980–2019. The dotted lines mark the correlation coefficient of +0.3, which is used as
 644 a threshold to define “moderate to high correlation”. The bar chart (right) represents the
 645 frequency of SLP and 500 hPa GPH anomalies in the same months during 1980–1999 (blue)
 646 and 2000–2019 (orange) that have moderate to high correlation (>0.3) with those in June 2018,
 647 July 2017, July 2015 and September 2019.

648



649

650 **Figure 9.** Frequencies of extreme months with T2m or RH anomalies exceeding the 80th
 651 percentile or below the 20th percentile of the distributions over NCP (115°–120°E, 38°–44°N)
 652 (a, b), YRD (120°–125°E, 28°–32°N) (c, d), SCB (102.5°–105°E, 30°–32°N) (e, f) and PRD
 653 (110°–115°E, 22°–26°N) (g, h) in each 10-year interval during 2021–2100 under two SSPs
 654 future scenarios of 13 CMIP6 models. The two SSPs are SSP1-2.6 and SSP5-8.5. The slope
 655 and P values of the linear regression during 2021–2100 are shown in the upper right of each
 656 panel.



657

658 **Figure 10.** Frequencies of extreme months with SLP and 500 hPa GPH that have moderate to
 659 high correlation (>0.3) to those in June 2018 (a, b), July 2017 (c, d), July 2015 (e, f) and
 660 September 2019 (g, h) in each 10-year interval during 2021–2100 under two SSPs future
 661 scenarios of 13 CMIP6 models. The two SSPs are SSP1-2.6 and SSP5-8.5. The slope and P
 662 values of the linear regression during 2021–2100 are shown in the upper right of each panel.
 663 The linear trends of SLP and GPH in each model grid were removed before the correlation
 664 coefficient is calculated.